Soft Matter

PAPER

View Article Online
View Journal | View Issue

Cite this: *Soft Matter*, 2018, **14**, 8580

Polymer functionalized nanoparticles in liquid crystals: combining PDLCs with LC nanocomposites†

Safiya Allie,[a] Ignacio Hegoburu,[b] Min Jeong Shin,[a] Jung Young Jung,[a] Violeta Toader,[a] Alejandro Rey,[c] Ezequiel R. Soule*[b] and Linda Reven *[a]

Received 11th June 2018,
Accepted 6th October 2018

DOI: 10.1039/c8sm01192c

rsc.li/soft-matter-journal

Liquid crystal (LC)–polymer blends are important stimuli responsive materials already employed in a wide range of applications whereas nanoparticle (NP)–LC blends are an emerging class of nanocomposites. Polymer ligands offer the advantages of synthetic simplicity along with chemical and molecular weight tunability. Here we compare the phase behavior of 5CB blended with poly(ethylene oxide) (PEO) and with gold NPs functionalized with thiolated PEO (AuNP–PEO) as a function of PEO concentration by DSC, POM and ^{13}C NMR spectroscopy. Both PEO and the AuNP–PEO form uniform dispersions in isotropic 5CB and phase separate below the I–N phase transition temperature. Above the PEO crystallization temperature, the PEO/5CB blends show the expected biphasic state of PEO rich-isotropic liquid co-existing with PEO-poor nematic droplets. At PEO concentrations above 10 wt%, nematic 5CB nucleates with PEO crystallization. Both PEO and AuNP–PEO induce homeotropic alignment of the 5CB matrix immediately below T_{NI}. The AuNP–PEO/5CB blends form thermally reversible cellular networks similar to AuNPs functionalized with low molecular weight mesogenic ligands. A thermodynamic model to account for the observed phase behavior is presented.

1. Introduction

Liquid crystal (LC)–polymer mixtures are materials that are stimuli responsive and often used in holographic films and displays. Polymers can be used to stabilize certain LC phases in addition to imparting flexibility and mechanical strength to LC-based materials. Since the 1960s, the phase behaviour and the electro-optical properties of polymer–LC blends have extensively been investigated. Despite recent improved characterization methods, many aspects regarding the nature of the interfaces in LC–polymer mixtures are still not well understood.[1,2]

Whereas liquid crystal–polymer blends are important stimuli responsive materials already employed in a wide range of applications, nanoparticle (NPs)–LC blends are an emerging class of nanocomposites.[3] LCs are advancing as dispersing mediums for NPs for the formation of dynamic nanostructures under thermal and electronic control. Local distortions of the LC director caused by NPs can result in spatial rearrangement of both the LC medium and NPs to reduce elastic perturbations. Other studies of NP–LC blends involve stabilization of LC phases, improving the LC electro-optical properties or electrical control of the nanoparticle optical or magnetic properties.[3–6]

The dispersion of gold NPs in LCs has been the subject of many studies due to the useful optical properties of gold NPs that can be functionalized with a wide range of ligands.[7] Milette *et al.* improved the miscibility of gold NPs using ligand exchange with 4-(*N*,*N*-dimethylamino)pyridine (DMAP) for thiol in 4-*n*-pentyl-4′-cyanobiphenyl (5CB) and 4-*n*-octyl-4′-cyanobiphenyl (8CB) LCs. Upon cooling, the isotropic–nematic transition produces a cellular network topology while the nematic–smectic transition consists of NPs phase separated into linear arrays. The dimensions of the topology of the cellular network in the nematic 5CB depends on the NP concentration, cooling rate and sample thickness whereas the boundary conditions (wedge cell *versus* a meniscus) determined the dimensions of the linear arrays of NPs formed at the nematic to smectic transition of 8CB.[8,9]

In contrast to the mesogenic ligands commonly used to produce homogeneous dispersions of nanoparticles in LCs,

[a] *Quebec Centre for Advanced Materials, Department of Chemistry, McGill University, 801 Sherbrooke St. W., Montreal QC H3A 0B8, Canada. E-mail: linda.reven@mcgill.ca*
[b] *Institute of Materials Science and Technology (INTEMA), University of Mar del Plata and National Research Council (CONICET), J. B. Justo 4302, 7600 Mar del Plata, Argentina*
[c] *Department of Chemical Engineering, McGill University, Montreal QC H3A 2B2, Canada*

† Electronic supplementary information (ESI) available: TEM and DSC of the pure AuNP–PEO, dispersions of AuNP–PEO in 5CB. Additional POM images and ^{13}C NMR of PEO and AuNP–PEO in 5CB. See DOI: 10.1039/c8sm01192c

polymer ligands offer chemical and molecular weight tunability and are relatively easy to synthesize. Recently, anisotropic plasmonic NPs functionalized with poly(ethylene oxide) (PEO) chains were shown to form stable dispersions in nematic LCs,[10–15] allowing electronic control of their plasmonic response. The dispersion of high concentrations of polymer functionalized NPs in liquid crystals presents an opportunity to characterize and understand the interactions between the NPs and the LC matrix at the molecular level by methods such as NMR spectroscopy.

This study aims to merge the fields of polymer dispersed LCs (PDLCs) and NP–LC blends by dispersing polymer functionalized gold NPs in LC matrices. In addition to producing LC composites with novel electro-optical properties, this approach may yield another route to reversibly template NPs into different spatial arrangements. The surface plasmon resonance of gold NPs provides a convenient method for detecting aggregation. Through variation of the molecular weight, the corona of polymer functionalized NPs provide another way to control the minimum spatial separation between the gold cores and thus the optical response. Furthermore, the doping of PDLCs by metallic NPs can enhance electro-optical properties such as the threshold voltage and switching speed for display applications.[16]

Here we compare the phase behaviour of 5CB blended with PEO and 5CB blended with PEO functionalized gold NPs. PEO was chosen as the polymer ligand due to previous success for producing stable NP–LC dispersions[10–15] and solubility in both water and organic solvents, which is useful since the precursor NPs are often prepared under aqueous conditions. The ligands and free PEO had the same molecular weight of 2000 mol g^{-1} and the dispersions were characterized as a function of PEO concentration by calorimetry, NMR and optical microscopy. The goals of this study are to (1) understand the effect of PEO alone and PEO tethered to NPs on the LC phase behaviour, (2) to determine the extent to which the spatial distribution of the NPs can be controlled and finally (3) the effect of crystallization of PEO.

Previous studies of polymer functionalized NPs in liquid crystals[10–15] are mostly low concentrations of large, anisotropic NPs with faceted surfaces expected to interact and anchor the LC molecules similar to polymer coated flat surfaces. There have been very few studies of PEO functionalized nanospheres[15] and none with the high concentrations required to detect molecular level interactions by spectroscopic techniques. Although PEO ligands have recently been used to stabilize NP–LC dispersions, there are very few studies of PEO–LC blends.[17–19] PEO is a semi-crystalline, low T_g polymer. Normally glassy, amorphous polymers rather than semi-crystalline polymers are used to make PDLCs and other types of polymer–LC blends. Therefore, the effect of a liquid crystalline solvent on the polymer crystallization is another unexplored topic.

2. Methods and techniques

Chemicals

Gold(III) chloride trihydrate (99.9%, MW = 393.83 g mol^{-1}), tetraoctylammonium bromide (98%, MW = 546.79 g mol^{-1}), sodium borohydride (99%, MW = 37.83 g mol^{-1}), 4-dimethylaminopyridine (99%, MW = 122.17 g mol^{-1}) were all purchased from Sigma Aldrich. The 2000 g mol^{-1} MW thiol terminated poly(ethylene glycol) methyl ether (2000 g mol^{-1} MW PEO-SH) was purchased from Polymer Source.

Synthesis of gold nanoparticles

The preparation of the gold nanoparticles functionalized with PEO was based on a procedure by Rucarneau *et al.*[20] All glassware was cleaned using aqua regia prior to use. 2 g of gold(III) chloride trihydrate was dissolved in 160 mL of Milli-Q water and poured in a 1 L round bottom flask. 12.24 g of tetraoctylammonium bromide dissolved in 400 mL of toluene was added and the mixture was vigorously stirred for 1 h. The bottom phase became clear after approximately an hour. Sodium borohydride dissolved in 120 mL of Milli-Q water was very slowly added and the solution was stirred for another 4 hours. The upper layer became a dark red and the aqueous phase was separated from the organic dark red phase. The organic phase was washed with Milli-Q water three times (3 × 70 mL). Anhydrous sodium sulfate was added and the solution was left overnight without stirring. The solution was filtered to remove the drying agent and toluene was used to dilute the total volume to 500 mL. After 6.1 g of 4-dimethylaminopyridine dissolved in 500 mL of Milli-Q water was added, the solution was left overnight. The aqueous phase at the bottom was kept while the organic layer was discarded. The solution was diluted to a total volume of 500 mL and stored in the refrigerator until further use.

The following procedure was used for the ligand exchange of DMAP for 2000 MW PEO-SH. The 500 mL gold was added to a round bottom flask and 2000 MW PEO-SH was dissolved in 500 mL Milli-Q water and slowly added. The solution is left to stir overnight. The mixture was concentrated using flowing air or a rotovap and dialysed against Milli-Q water at least three times. The PEO and the AuNP–PEO were thoroughly dried at 60 °C under vacuum to remove water before dispersing in 5CB LC using the co-solvent method.

Characterization

Polarized optical microscopy (POM). All glass slides were treated with *aqua regia* and rinsed with water, acetone and hexane prior to use. The microscope used was the Nikon Eclipse LV100POL optical microscope with 5 × magnification. A Mettler FP52 heating plate was used to vary the temperatures of the liquid crystal dispersions between the isotropic, nematic and crystallization phases. After heating to the isotropic phase of 5CB, a cooling rate of 1 deg min^{-1} was used for all the samples.

NMR spectroscopy. 125.71 MHz ^{13}C NMR spectra were acquired using a 500 MHz Varian VNMRS spectrometer equipped with a 5 mm inverse liquids NMR probe. At each temperature, 64 transients were acquired with a recycle delay of 6 s using an excitation pulse of 9.9 μs followed by SPINAL decoupling at approximately 15 kHz. Spectra of both the 5 wt% PEO/5CB and 30 wt% PEO/5CB samples were acquired at 0.3 °C

temperature increments between 45 °C and 18 °C. Spectra of the 10 wt% AuNP–PEO/5CB and 50 wt% AuNP–PEO/5CB samples were acquired at 0.5 °C increments between 36 °C to 18 °C, allowing a temperature equilibration delay of 180 s between temperatures.

Differential scanning calorimetry (DSC). All DSC experiments were done using the DSC Q2000, TA Instruments. The samples were initially equilibrated at −40 °C and set to undergo 6 cycles. Cycles 1, 3, 5 were done by heating at 1 °C min^{-1} from −40 °C to 100 °C while cycles 2, 4, 6 were done by cooling at 1 °C min^{-1} from 100 °C to −40 °C.

Thermogravimetry analysis (TGA). All TGA experiments were done using the TGA Q500, TA Instruments. From room temperature up until 550 °C nitrogen gas was used and from 550 °C up until 700 °C it was switched to synthetic air. These experiments were done at a rate of 20 °C min^{-1}. A sample size of 3–10 mg was used.

3. Results and discussion

Gold nanoparticles (AuNPs), with an average diameter of 4.5 nm and functionalized with thiolated polyethylene oxide (PEO-SH, MW 2000 g mol^{-1}) ligands (AuNP–PEO), were synthesized and dispersed in the nematic liquid crystal 4-*n*-pentyl-4′-cyanobiphenyl (5CB). Concentrations of 1, 10, 20 and 50 wt% AuNP–PEO in 5CB were prepared and characterized by polarized optical microscopy (POM) and differential scanning calorimetry (DSC). Given that the PEO ligands constitute ∼68% of the weight of the AuNP–PEOs, this corresponds to loadings of ∼3, 6 and 16 wt% Au which are very high as compared to most studies of LCs doped with gold nanoparticles. The corresponding PEO contents are 0.5, 6.8, 13.6 and 34 wt%. To compare the effect of free PEO *versus* PEO tethered to gold NPs on the LC properties, dispersions of PEO (MW 2000 g mol^{-1}) in 5CB were also prepared.

3.1 Optical microscopy

First the POM images of the blend with the highest NP concentration, 50 wt% AuNP–PEO in 5CB, in Fig. 1 and 2, are discussed in detail. The PEO functionalized AuNPs were observed to be uniformly dispersed in isotropic 5CB, even for the highest concentration of 50 wt% AuNP–PEO (Fig. 1a and b) with no visible aggregates on the micron scale. The intense red color in the images without crossed polars (Fig. 1a and d) arises from the surface plasmon resonance ($\lambda \sim 520$ nm) of ∼4.5 nm dia. gold NPs. In addition to the good miscibility with isotropic 5CB, the polymer corona of PEO chains, which in water is estimated to have a thickness of ∼6 nm[21] plays a role in preventing small core–core distances that would cause a shift in the surface plasmon resonance to higher wavelengths. Likewise, the dispersion of 30 wt% PEO in 5CB, which is close to the 34 wt% PEO content for the 50 wt% AuNP–PEO dispersion, is completely miscible in isotropic 5CB (Fig. 1c, f and i).

The following description of the POM images as the nanocomposite is cooled from the isotropic phase is aided by earlier studies by Milette *et al.* for gold NPs of the same size but functionalized with low molecular weight mesogenic ligands.[8] Upon cooling at a rate of 1 °C min^{-1} to the isotropic–nematic transition, Maltese crosses begin to form uniformly in the black isotropic LC (Fig. 1d and e) as the nematic droplets nucleate. By examining the images with and without cross polars, it can be concluded that the AuNPs concentrate into the remaining isotropic 5CB which becomes darker in the images without cross polars. Such partitioning is expected as the elastic forces of the LC phase will tend to expel the NPs into regions of disordered LC and can often result in a complete bulk phase separation.

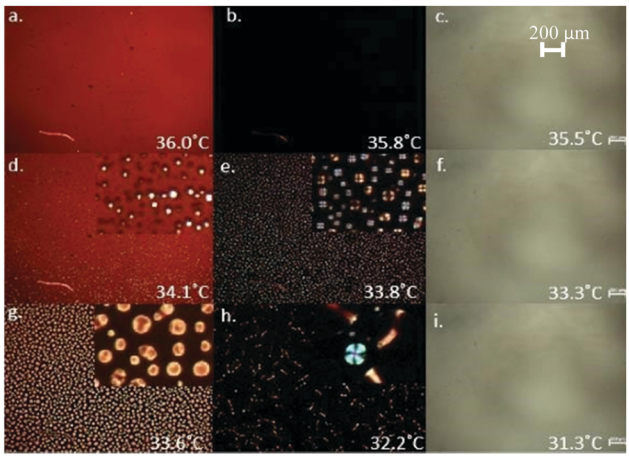

Fig. 1 POM images of 50 wt% of Au-NPs/PEO LC dispersion at different temperatures using a cooling rate of 1 °C min^{-1}. Images viewed with no analyzer are shown in a, d, g and with crossed polarizers are shown in b, e, h. The inset of images d, e, g, h is an enlarged area of each respective texture. The corresponding POM images of 30 wt% PEO/LC dispersion are shown in c, f, i viewed with crossed polarizers under more light to detect any I–I phase separation.

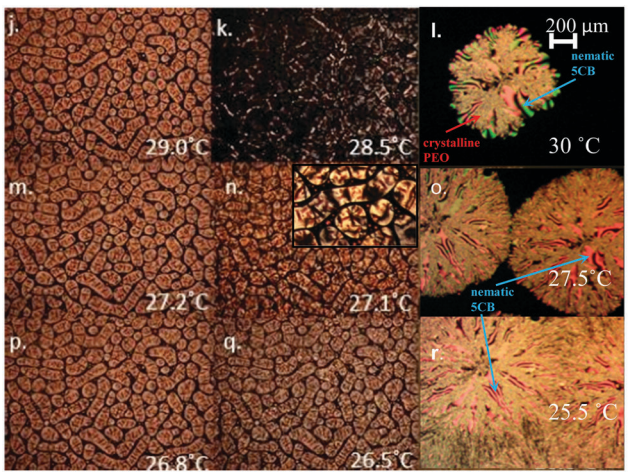

Fig. 2 POM images of 50 wt% of Au-NPs/PEO LC dispersion at different temperatures using a cooling rate of 1 °C min^{-1}. Images with no analyzer are shown in j, m, p and with crossed polarizers are shown in k, n, q. The corresponding POM images of 30 wt% PEO/LC dispersion are shown in l, o, r using crossed polarizers. The inset of images n and q is an enlarged area of each respective texture.

In Fig. 1g, an image of the 50 wt% AuNP/5CB blend without cross polars, the isotropic regions around the nematic droplets are dark due to the high concentration of AuNPs. Light cannot get through due to the very high density of gold NPs. The nematic droplets are a lighter red color, indicating a lower concentration of AuNPs within these droplets. Under the cross polars, the nematic droplets become black (Fig. 1h) shortly after the phase transition due to homeotropic alignment induced by the AuNPs, a phenomenon previously observed for AuNPs with low molecular weight ligands dispersed in 5CB.[8,22] The homeotropic alignment results in dark areas under crossed polars because the director of the liquid crystal molecules is uniformly perpendicular to the glass surface. In the absence of NPs, the usual nematic texture is observed on the acid-washed glass slides.[8] The NPs tend to concentrate at the surfaces and act as surface alignment layers, a thermally reversible process.[22] Within the growing and merging nematic droplets, a cellular network, consisting of branches that are regions of LC with more concentrated AuNPs, is formed accompanied by birefringent stripes. This is seen in the images without the cross polars where there are dark red lines due to a higher concentration of AuNPs (Fig. 1g) within the nematic droplets. The birefringent stripes, which are frequently observed for nanoparticle dispersions in nematic LCs, are metastable twist disclination lines located at the surfaces that are stabilized by NPs (Fig. 1h).[8,23]

Next the evolution of the 50 wt% AuNP/5CB dispersion as the temperature is further lowered in the nematic phase are presented in Fig. 2. The observed textures continue to be very similar to the AuNPs with low molecular weight ligands. At 28.5 °C (Fig. 2k) the homeotropic regions begin to disappear and the usual nematic Schlieren texture appears.[24] This is presumably due to the continued migration of the AuNPs into the branches of the cellular network. Such a change was also observed in the cellular network formed by AuNPs with mesogenic ligands in 5CB that was left to anneal overnight.[8] At 27.1 °C, all the homeotropic alignment is gone and dark branches due to the concentrated AuNPs are now visible with the cross polars. Presumably there could be also isotropic 5CB within these branches as observed by ^{2}H NMR for the cellular networks formed by the AuNPs with short mesogenic ligands.[25] Since both the concentrated AuNPs and isotropic 5CB appear black under cross polars, POM cannot not be used to detect a biphasic state, that is the coexistence of isotropic and nematic liquid. Therefore a possible biphasic state was investigated by ^{13}C NMR as described later.

At 26.5 °C, there is a change in the birefringence in the regions between the dark branches (Fig. 2q). Upon close examination, the new texture, that appears to be polycrystalline in nature, is superimposed upon the nematic texture. (See ESI† for enlarged images, Fig. S1). We attribute this change in the birefringence to crystallization of the PEO ligands of the AuNPs remaining in the 5CB droplets as it occurs in the same temperature range as the crystallization of a similar concentration of PEO in 5CB. The PEO crystallization temperature due to supercooling is highly dependent on the cooling rate that was kept at 1 °C min^{-1} for the DSC runs. The PEO ligands of dry AuNP–PEO crystallize at ~30 °C and dry PEO, MW 2000 g mol^{-1}, crystallizes at 34 °C. (ESI,† Fig. S5 and S6) In the dark branches where the AuNP–PEOs are highly concentrated, it cannot be determined by POM whether polymer crystallization also occurs in these regions. However non-crystalline PEO chain segments are detected by ^{13}C NMR as described later.

We note that the I–N transition temperature, that is, the initial appearance of nematic 5CB droplets, is not significantly affected by the high concentration of AuNPs whereas adding free PEO at the equivalent concentration (30 wt% PEO) lowers the nematic nucleation temperature of 5CB by a few degrees. Interestingly, the lowering of the I–N transition temperature of 5CB and the PEO crystallization temperature results in the simultaneous nucleation of nematic liquid and PEO crystallization for concentrations between 30 and 10 wt% PEO. The nucleation of nematic liquid with PEO crystallization may also occur for concentrations above 40 wt% PEO, however, it is difficult to detect by POM. In Fig. 2l, o and r, nematic liquid is visible at the borders and between the branches of a growing PEO dendritic crystal that evolves into a spherulite as the crystallization proceeds. (See ESI† for enlarged image, Fig. S2).

Milette *et al.* reported that nanoparticle network formation is due to the LC elastic and particle–particle forces and is dependent upon the cooling rate, nanoparticle concentration and the sample thickness.[8] To examine the effect of particle concentration, 20, 10, 5.0 and 1.0 wt% Au–PEO/5CB dispersions were studied. The POM images and detailed description of the 10 and 1 wt% AuNP–PEO in 5CB are found in the ESI,† (Fig. S3–S6). Like the AuNPs with mesogenic ligands, AuNP–PEO NP cellular network dimensions increase with decreasing particle concentration and birefringent stripes and homeotropic alignment again observed for the lower particle concentrations.

In corresponding PEO/5CB blends (5 and 0.5 wt%) the nematic droplets appear at higher temperatures while the PEO crystallizes at lower temperatures under the same cooling rates. With decreasing polymer concentration, the morphology of the crystallites becomes dendritic, similar to PEO crystallization in polymer blends and in thin films.[26] A biphasic state is present where the nematic LC co-exists with isotropic liquid that has a higher concentration of PEO. Such phase behaviour and partitioning is commonly observed in polymer–liquid crystal blends.[1] The assumption that the PEO concentrates into the isotropic liquid is clearly revealed with the PEO crystallites visibly forming in the remaining regions of isotropic 5CB (Fig. S2r, ESI†). This biphasic behaviour is quantitated by ^{13}C NMR spectroscopy as presented later.

3.2 Differential scanning calorimetry

In general, the phase transitions detected by calorimetry are consistent with the changes detected by POM. The PEO crystallization and I–N transition of 5CB observed by POM were only detected by DSC when the composites contain sufficient quantities of either component. The PEO crystallization peak is only large enough to be detected in the 50 wt% AuNP–PEO dispersion in 5CB. The I–N transition is also visible in the AuNP/5CB blends but is broadened as compared to pure 5CB (ESI,† Fig. S7 and S8).

For the PEO dispersions in 5CB, the I–N transition is only sufficiently separated from the PEO crystallization peak to be visible for concentrations below 10 wt% PEO. At higher PEO concentrations, the I–N phase transitions and PEO crystallization coincide according to the POM data that was acquired with the same cooling rate of 1 deg min^{-1}.

3.3 ^{13}C NMR spectroscopy

The nematic order parameter and the fraction of remaining isotropic liquid were measured by ^{13}C NMR, similar to a study of polymer dispersed liquid crystals (PDLC) where the LC was also 5CB.[27] ^{13}C spectra comparing the 50 and 10 wt% AuNP–PEO and the 30 and 5 wt% PEO dispersions in 5CB that are comparable in terms of PEO content are given in the ESI,† Fig. S9.

The observations regarding the PEO NMR signal will be described first. Whereas the PEO peak at 74 ppm is detected for both the 30 and 5 wt% PEO and the 50 wt% AuNP–PEO in 5CB, the signal is below the detection limit for the 10 wt% AuNP–PEO in 5CB. The disappearance of the PEO peak is attributed to the onset of crystallization that depends on the degree of supercooling. The ^{13}C spectra were collected at intervals of 0.3 or 0.5 degrees after equilibrating, a slower cooling rate than the 1 °C min^{-1} was used for the POM and DSC experiments. This difference in the cooling rates could result in PEO crystallization occurring at a higher temperature in the NMR as compared to the POM and DSC experiments. The integrated intensities of the PEO ^{13}C NMR signal as a function of temperature are presented in Fig. 3.

In the ^{13}C NMR spectrum of the 30 wt% PEO in 5CB (ESI,† Fig. S9a), the PEO peak at 74 ppm is narrow as expected since the PEO is completely soluble in isotropic 5CB. At ~38 °C, which is higher than the temperature where crystallization is observed by POM (T_C ~ 30 °C), the PEO peak intensity rapidly diminishes (Fig. 3). In the POM measurements, polymer crystallization and nucleation of nematic liquid occur simultaneously for polymer concentrations above 10 wt% PEO. (Fig. 2). In the NMR experiment with less supercooling, PEO begins crystallizing before the nematic 5CB peaks appear at T_{NI} ~ 32 °C for the 30 wt% PEO dispersion (ESI,† Fig. S9a).

In the 5 wt% PEO dispersion, the NMR peaks for nematic 5CB appear at a higher temperature than the PEO crystallization (ESI,† Fig. S9c). This lower polymer concentration does not significantly lower the 5CB phase transition temperature, T_{NI} ~ 34 °C, but the PEO crystallization, as indicated by the disappearance of the NMR peak (ESI,† Fig. S9c) occurs at a lower temperature, ~30 °C, as compared to the 30 wt% PEO concentration (~38 °C). Thus the 74 ppm PEO peak, albeit weak due to the low PEO concentration, persists at temperatures far below the appearance of nematic 5CB. This signal is presumably associated with PEO chains concentrated in the remaining isotropic 5CB and is consistent with the POM images that clearly show that the PEO crystallization occurs in the regions of remaining isotropic liquid (ESI,† Fig. S4r). This interpretation is supported by the measurement of the nematic fraction as discussed below.

The temperature dependence of the PEO signal of the nanoparticles is described next. The 74 ppm peak for PEO ligands bound to the AuNPs is significantly broader than the free PEO, even in the isotropic 5CB (ESI,† Fig. S9). Due to reduced mobility, it is possible that not all the PEO ligand chain segments are observed because their signals are broadened into the baseline. The possibility of free PEO ligands being associated with this component can be excluded due to the rigorous purification of the AuNPs after ligand exchange. Unlike the 30 wt% PEO, the 50 wt% AuNP–PEO peak broadens but remains visible (ESI,† Fig. S9b) even as the corona of PEO ligands presumably crystallize as observed by POM (Fig. 2r and Fig. S1, ESI†). In contrast to the 30 wt% PEO, where PEO crystallization and nucleation of nematic 5CB coincide, the POM images indicate that nematic 5CB appears before crystallization of the PEO ligands, even for the highest concentration of AuNP–PEO. This shows that the PEO ligand chain dynamics are influenced mostly by the chain packing as dictated by tethering to a high curvature surface. Whereas the intensity of the free PEO signal abruptly diminishes with crystallization, the PEO chains bound to the AuNPs cannot completely crystallize and a gradual decrease in intensity with temperature is observed instead. (Fig. 3)

The effect of the polymer and AuNP additives on the 5CB orientational order are presented. The order parameter was calculated from the ^{13}C chemical shifts using the following semi-empirical equation from ref. 27 for 5CB:

$$S = \frac{\Delta\delta}{a} - \frac{b}{a}$$

$\Delta\delta$ is the observed chemical shift, b is an empirical constant and $a = 2\Delta\sigma/3$ is calculated from the chemical shift anisotropy, $\Delta\sigma = [\sigma_{zz} - 1/2\ (\sigma_{xx} + \sigma_{yy})]$ of the particular carbon site. The order

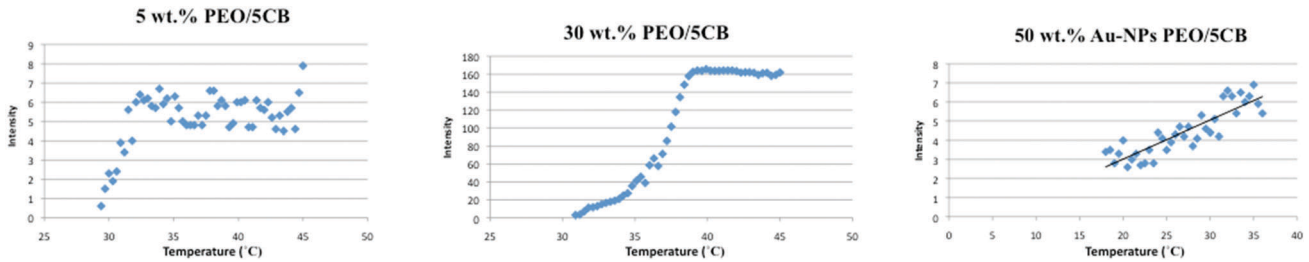

Fig. 3 Integrated intensities of the ^{13}C NMR peak at 74 ppm from the PEO chains as a function of temperature.

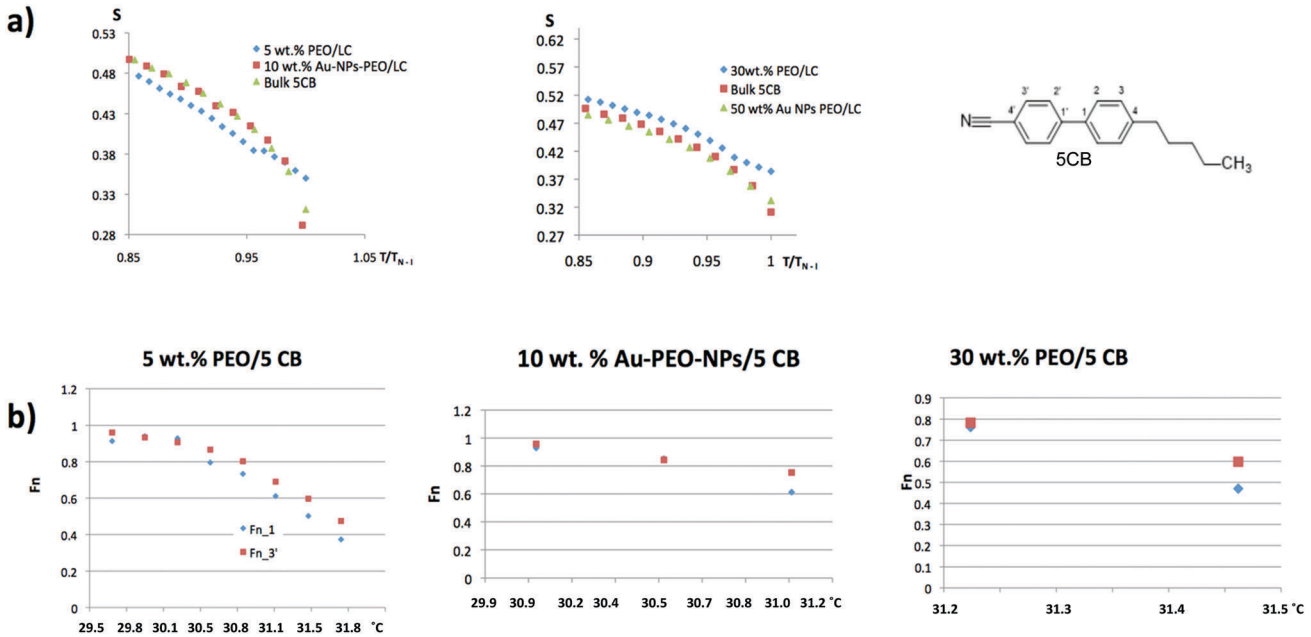

Fig. 4 (a) Order parameter and (b) nematic fractions of 5CB for the indicated PEO and AuNP–PEO dispersions as a function of temperature.

parameter, S, of the 5CB matrix was calculated from the eight carbons as indicated on Fig. 4.

In Fig. 4a, the order parameters of the dispersions are compared with pure 5CB close to T_{NI}. The effect of PEO alone as a function of concentration on the LC orientational order is consistent with previous studies.[27] At the higher 30 wt% concentration, the order parameter is higher than that of 5CB which can be attributed to confinement effects whereas for the 5 wt% PEO concentration the order parameter is lower due to dilution effects. By contrast, the AuNP–PEO additive has little effect on the order parameter, even at the highest concentration.

Finally the nematic fractions, $F_N = I_N/(I_N + I_I)$, were calculated from the intensities of the isotropic and nematic ^{13}C peaks for carbon sites 1 and 3′ which have nematic ^{13}C chemical shifts that are well resolved from the other sites (Fig. 4b). This NMR data confirms the formation of a biphasic state in the presence of free PEO with polymer-rich isotropic phase and polymer-depleted nematic phases, in agreement with the literature. The temperature range of the biphasic state is larger for the lower concentrations of PEO and AuNP–PEO. The biphasic region, consisting of polymer-rich isotropic liquid and polymer-depleted nematic liquid, normally increases with increasing polymer concentration. In the case of the 30 wt% PEO in 5CB, the lack of a significant biphasic region is due to the PEO crystallization near T_{NI} that results in the complete expulsion and phase separation of the PEO from the 5CB. No biphasic region was observed by NMR for the 50 wt% AuNP–PEO dispersion. A small biphasic state is observed by POM but the origin may be different as shown by the appearance of PEO crystallites throughout the cellular network (Fig. S1, ESI†). This may be due to the non-complete PEO crystallization when the polymer is grafted to AuNPs. The ^{13}C NMR signals of any remaining isotropic 5CB within the PEO coronas of the AuNPs may be broadened beyond detection due to reduced mobility.

3.4 Thermodynamic modeling

In order to understand the experimental observations, the phase diagrams for the PEO alone and AuNP–PEO in 5CB were constructed based on the thermodynamic models previously developed for polymer and nanoparticle dispersions in simple nematic liquid crystals.[28]

3.4.1 Phase diagram for PEO in 5CB. The dimensionless free energy per mole of cells for an isotropic or nematic phase of the PEO/5CB blend is expressed according to Flory–Huggins and Maier–Saupe theories as:[28]

$$\frac{F_{\text{liquid}}}{MRT} = \frac{\phi_{PEO}}{r_{PEO}}\ln\phi_{PEO} + \frac{\phi_{5CB}}{r_{5CB}}\ln\phi_{5CB} + \chi\phi_{PEO}\phi_{5CB} + \frac{\phi_{5CB}}{r_{5CB}}\left(\frac{1}{2}\nu\phi_{5CB}S^2 - \ln Z\right) \quad (1)$$

where ϕ is the volumetric fraction, r is the dimensionless volume, expressed in terms of the number of cells occupied by a component, $\chi = B/T$ is the mixing interaction parameter, $\nu = 4.54T_{NI,5CB}/T$ is the nematic quadrupolar interaction parameter, and $T_{NI,5CB}$ the nematic–isotropic transition temperature of pure 5CB. The partition function Z is well-approximated with a polynomial function of the order parameter.[29] The crystalline phase is assumed to be pure PEO, and if the change in enthalpy and entropy of crystallization with temperature is neglected, the free energy is:

$$\frac{F_{\text{crystal}}}{MRT} = \frac{\Delta H_{\text{crys}}}{MR}\left(\frac{1}{T} - \frac{1}{T_{\text{crys}}}\right) \quad (2)$$

The geometrical/molecular parameters consist of a reference length of 0.53 nm (reference volume = $[0.53\text{ nm}]^3$) and a cylindrical shape

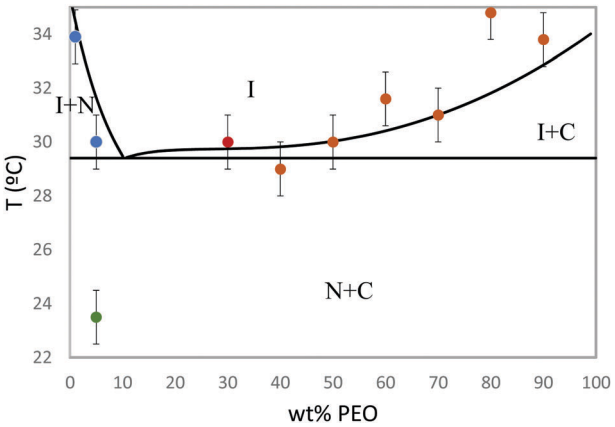

Fig. 5 Phase diagram and phase transition for PEO/5CB. The phase or phases existing in each region of the calculated phase diagram are indicated (I: isotropic, N: nematic, C: crystal). The black lines represent calculated phase boundaries and crossing each line correspond to a phase transition. Full lines correspond to equilibrium phase transition. Circles indicate experimental phase transitions as observed by POM (blue: I to I + N, green: I + N to C + N, red: I to N + C, orange: I + I + C).

for 5CB with an effective diameter of 0.53 nm, a 3.5 aspect ratio, a non-dimensional volume of 2.7489 and T_{NI} = 35.4 °C. For PEO (MW 2000 g mol^{-1}, density 1.124 g m^{-3}), a non-dimensional volume of 19.8466 and ΔH_{cryst} = 200 J g^{-1} = 4800 J per cell were used. The interaction parameter B was the only adjustable parameter in the model.

Fig. 5 shows the calculated phase diagram with B = 102, and the experimentally observed phase transitions. The model predicts that the nematic phase is essentially pure 5CB while the isotropic phase contains both 5CB and PEO. The experimental results are very well represented by the calculated phase diagram; note that the difference between the experimental and predicted results for I to I + N and for I to N + C transitions is only 1–2 °C. For 30 wt% PEO in 5CB, where the I to N + C transition is experimentally observed, the model predicts a sequence I to C + I to N + C, but it is noted that C + I coexistence would be observed in a very narrow temperature range. Crystallization is a relatively slow process so when a cooling temperature ramp is applied, the appearance of crystals is expected to require some degree of supercooling to be observed. Thus the C + I coexistence can be easily missed. A larger discrepancy is observed for PEO crystallization in the 5 wt% mixture, where the experimental crystallization temperature is 23 °C, but the model predicts the equilibrium transition at 29.3 °C. As discussed previously, some degree of supercooling is necessary for the formation of crystalline phase in the mixture with 30 wt% PEO but the required supercooling is much larger for 5 wt% PEO (it has to be noted that, as mentioned in Section 3.3, in NMR experiments, where a slower cooling rate was used and a smaller supercooling for crystallization was observed).

Although the phase equilibrium diagram is not enough to quantitatively predict the phase transition mechanism and the final morphology, it can be used to qualitatively explain some experimental observations. In order to do that, some metastable states have to be considered as crystallization, being a slow process, requires supercooling and thus is an out of equilibrium process. Fig. 6 shows the phase diagram again but the I + C and I + N phase coexistence regions extended into the N + C region. Here the N + C coexistence represents the true equilibrium, while I + C and I + N coexistence are metastable states. The blue arrow represents the trajectory followed by the 30 wt% PEO mixture when it is cooled down from the isotropic phase. It first meets the I + C phase transition, but as mentioned before, crystallization is slow and the I + C region spans a narrow temperature range, so the isotropic mixture enters the N + C region before crystals are formed. As the mixture is further cooled and supercooling increases, supersaturation (which is the length of the horizontal blue lines in Fig. 6) increases very sharply, because the I + C boundary is almost horizontal in this compositional range. This implies a very large increase of the driving force for crystallization, such that a relatively small (but not negligible) supercooling is enough to nucleate the crystal phase. When this happens, 5CB is expelled from the crystal (which is pure PEO) and accumulates next to the interface of the crystals. The interface of the crystal is at (or close to) equilibrium (in this case, the metastable I + C equilibrium), which means that the isotropic phase at the crystal interface is saturated in PEO and thus follows the I + C (metastable) coexistence boundary. This is indicated by the blue dot in Fig. 6. Note that this isotropic phase is within the metastable I + N coexistence region, and the formation of a nematic phase is much faster than crystallization. Consequently, as soon as crystals are formed, the nematic phase is nucleated in the vicinity of their interface, as observed experimentally.

In the case of 5 wt% PEO, when this mixture is cooled (green arrow in Fig. 6) first the I to I + N transition is observed. The I + N phases are in equilibrium (or close to it), and when the N + C region is reached, I + N phases remain in metastable equilibrium. Now there is a driving force for the nucleation of a crystalline phase, given by the supersaturation (shown as

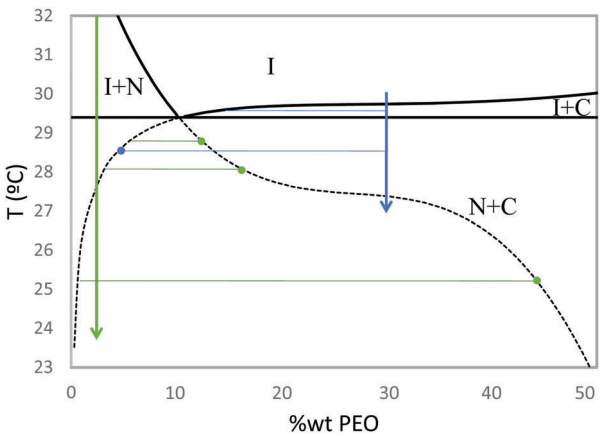

Fig. 6 Phase trajectories for mixtures with different PEO content: 5 wt% (green) and 30 wt% (blue). Phase diagram is shown as in Fig. 5, in addition, the metastable regions of I + N and I + C phase equilibrium are shown. Horizontal lines represent the supersaturation of the isotropic phase (*i.e.* the distance to the crystal branch of the I + C coexistence).

green horizontal lines) of this metastable isotropic phase (shown by green dots). Note that the supersaturation increases much slower with supercooling in this case, when compared to the 30 wt%, which implies a smaller (or, more precisely, more slowly growing) driving force for crystallization. In addition, the crystal is more difficult to nucleate because the PEO content of the isotropic phase is smaller (at least in some of the temperature range), so a larger composition fluctuation is required. That is why a much larger super-cooling is needed to observe crystallization in this mixture.

Finally, in Fig. 7, the predicted and experimental values of the fraction of 5CB in the nematic phase are shown. The agreement is reasonable if the horizontal distance between prediction and experiments is considered since the maximum difference is only ~ 2 °C.

3.4.2 Phase diagram for AuNP–PEO in 5CB. The dimensionless free energy per mole of cells is expressed according to our model based in Flory–Huggins, Maier–Saupe and Carnahan Starling theories,[28] and considering that interactions are proportional to the area fractions, as:

$$\frac{F_{\text{liquid}}}{\text{MRT}} = \frac{\phi_{\text{NP}}}{r_{\text{NP}}}\ln\phi_{\text{PEO}} + \frac{\phi_{\text{5CB}}}{r_{\text{5CB}}}\ln\phi_{\text{5CB}} + \frac{\phi_{\text{NP}}\left(4\phi_{\text{NP}} - 3\phi_{\text{NP}}^2\right)}{r_{\text{NP}}\quad\left(1-\phi_{\text{NP}}\right)^2} + \chi a_{\text{NP}}\phi_{\text{NP}}\varphi_{\text{SCB}} + \frac{\phi_{\text{5CB}}}{r_{\text{5CB}}}\left(\frac{1}{2}\nu\varphi_{\text{5CB}}S^2 - \ln Z\right) - wr_{\text{5CB}}a_{\text{NP}}\phi_{\text{NP}}\varphi_{\text{5CB}}S^2 \quad (3)$$

where a_{NP} represents the dimensionless surface area of NPs (considered as solid spheres), φ is the area fraction, and w is a binary nematic interaction parameter. The same parameters as before were used for 5CB along with a nanoparticle radius of 8.25 nm (2.25 nm of gold core and 6 nm of PEO corona thickness). The phase diagram of the AuNP–PEO/5CB mixtures is shown in Fig. 8. Only the N + I coexistence was calculated, because modeling PEO crystallization within the NP corona would require a much more complex model. First, an attempt was made to reproduce the experimental results without any adjustable parameter, using the same interaction parameter that was found in the case of PEO–5CB, but this was not possible. It was necessary to introduce a non-zero value of the binary nematic interaction parameter w. As seen in Fig. 8, a good fitting is obtained when $w = -160/T$. This means that, when PEO is present in the corona of the nanoparticle, there exists a specific interaction that favors the formation of a nematic phase that is not present in the case of non-bonded PEO. It is interesting to note that the model predicts a very narrow temperature range of phase coexistence, barely distinguishable in Fig. 8. Although coexistence is observed experimentally, it can be seen in the micrographs that the nematic domains grow very fast with decreasing temperature, and a network structure is rapidly observed. The domain walls in this network might be the remaining isotropic phase (in small amount), or some type of defect wall. For the case of the 1 wt% NPs, the network disappears and only some spherical domains remain (seen at 31.5 °C with crossed polarizers, ESI,† Fig. S6), this seems to be a small amount of remaining isotropic phase. This is not captured by our model, that predicts a homogeneous nematic phase. But the fact that, experimentally, the amount of the nematic phase increases faster with decreasing temperature in the case of AuNP–PEO/5CB than for PEO–5CB, seems to indicate that the coexistence region is smaller for the NP system; this trend is qualitatively captured by the model. In order to better reproduce the experimentally observed N + I phase coexistence, a larger value of B (from the isotropic interaction parameter), could be used. But a very large value (much larger than for the PEO–5CB system) is required to modify the phase behavior (which would imply immiscibility for PEO–5CB). Clearly, our simple model can capture some significant experimental trends, but there seems to be some additional factors that we are missing that will require a more sophisticated analysis. For example, polydispersity in NP size (this could arise not only from a polydispersity in the size of the metallic core; it is expected that there is some dispersion in the number of ligands per particles as well), or the presence of a small amount of free PEO desorbed from the NP surface, might lead to a fraction with lower solubility in 5CB and broaden the range of phase coexistence. In addition, the model makes some important simplifications, such as considering the particles as hard

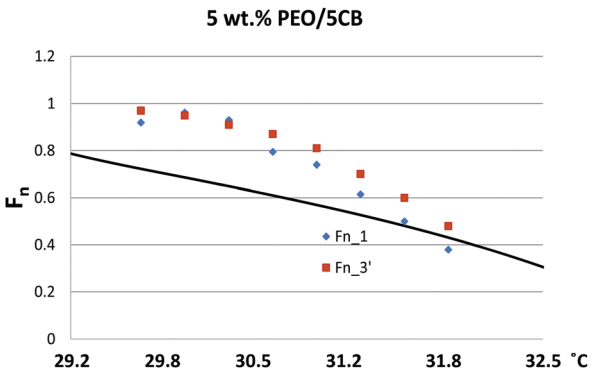

Fig. 7 Fraction of 5CB in the nematic phase predicted (black line) compared to the experimental data.

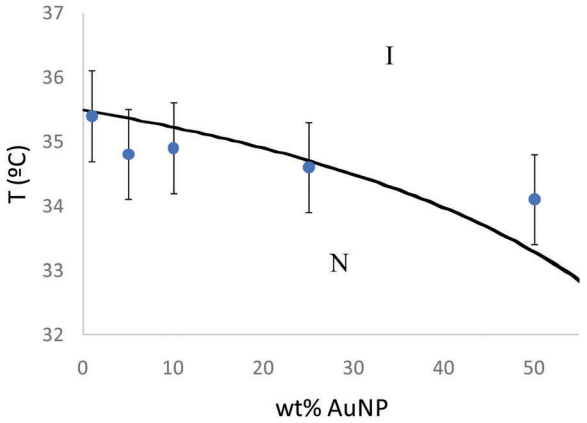

Fig. 8 Phase diagram of AuNP–PEO/5CB mixtures.

spheres, but the softness of the PEO corona can introduce additional physical phenomena. Developing such complex models is beyond the scope of this theory and simulation work.

4. Summary

The properties of gold NPs with polymer ligands blended with a simple nematic were characterized by POM, DSC and ^{13}C NMR and compared to the analogous polymer/LC blends and dispersions of the same gold NPs with mesogenic ligands. The PEO/5CB blends show the expected characteristics of a flexible, random coil polymer in a nematic solvent. The PEO partially phase separates into a biphasic state at the isotropic–nematic phase transition into polymer-rich isotropic liquid and polymer poor nematic droplets. At higher PEO concentrations nematic liquid is observed to nucleate at the interfaces of the growing polymer crystallites.

Despite the large difference in the ligand structures, the AuNPs with polymer ligands show similar behaviour to those with mesogenic ligands with regards to their effect on the nematic matrix: thermally reversible homeotropic alignment, meta-stable line defects, and little effect on the LC order parameter or phase transition temperatures. Both types of AuNPs are miscible to very high concentrations in isotropic 5CB and form thermally reversible cellular networks at T_{NI}. The differences in the network morphologies and presence of isotropic liquid below T_{NI} is related to the different ligand shell thicknesses and the extent to which the 5CB molecules can penetrate these shells.

A previously developed thermodynamic model was able to explain the experimentally observed phase behaviour of low molecular weight PEO in 5CB, including the simultaneous appearance of two ordered phases: nematic 5CB and crystalline PEO. Likewise, the basic features of phase diagram for the PEO functionalized AuNPs were produced but further development of the thermodynamic model in conjunction with molecular modelling is required to capture features such as a wide N + I region and crystallization within the polymer corona.

Depending on the application, this study shows that polymer functionalized NPs may offer a useful alternative to using custom-synthesized mesogenic ligands to prepare liquid crystal nanocomposites. For spectroscopic characterization purposes, only very high particle concentrations were examined here. Future studies, in addition to lower particle concentrations, will examine whether tuning the ligand shell by molecular weight, chain density by adding short spacer ligands and/or chain stiffness by using rigid-rod type polymers, can improve the colloidal stability of polymer functionalized nanoparticles in liquid crystal solvents.

Conflicts of interest

There are no conflicts to declare.

Acknowledgements

Funding for this research was provided by Fonds quebecois de la recherche sur la nature et les technologies (FQRNT) and the Natural Sciences and Engineering Research Council of Canada (NSERC). A. D. R. is thankful to McGill University for financial support through the James McGill Professorship appointment.

Notes and references

1 M. Mucha, *Prog. Polym. Sci.*, 2003, **28**, 837.
2 S. Bronnikov, S. Kostromin and V. Zuev, *J. Macromol. Sci., Part B: Phys.*, 2013, **52**, 1718.
3 J. P. F. Lagerwall and G. Scalia, *Liquid Crystals with Nano and Microparticles*, World Scientific Publishing, Singapore, 2017.
4 C. Blanc, D. Coursault and E. Lacaze, *Liq. Cryst. Rev.*, 2013, **1**, 83.
5 G. Si, Y. Zhao, E. S. Leong and Y. J. Liu, *Materials*, 2014, **7**, 1296.
6 M. Bagiński, A. Szmurło, A. Andruszkiewicz, M. Wójcik and W. Lewandowski, *Liq. Cryst.*, 2016, **43**, 2391.
7 A. Choudhary, G. Singh and A. M. Biradar, *Nanoscale*, 2014, **6**, 7743.
8 J. Milette, S. J. Cowling, V. Toader, C. Lavigne, I. M. Saez, R. B. Lennox, J. W. Goodby and L. Reven, *Soft Matter*, 2012, **8**, 173.
9 J. Milette, V. Toader, L. Reven and R. B. Lennox, *J. Mater. Chem.*, 2011, **21**, 9043.
10 Q. Liu, Y. Yuan and I. I. Smalyukh, *Nano Lett.*, 2014, **14**, 4071.
11 B. Senyuk, G. David and I. I. Smalyukh, *Phys. Rev. E: Stat., Nonlinear, Soft Matter Phys.*, 2013, **88**, 062507.
12 G. H. Sheetah, Q. Liu and I. I. Smalyukh, *Opt. Lett.*, 2016, **41**, 4899.
13 Q. Wang, L. Liu and L. Xu, *RSC Adv.*, 2018, **8**, 4104.
14 M. R. Thomas, J. E. Hallett, S. Klein, S. Mann, A. W. Perriman and R. M. Richardson, *Mol. Cryst. Liq. Cryst.*, 2015, **610**, 44.
15 A. W. Hauser, D. Liu, K. C. Bryson, R. C. Hayward and D. J. Broer, *Macromolecules*, 2016, **49**, 1575.
16 A. Hinojosa and S. C. Sharma, *Appl. Phys. Lett.*, 2010, **97**, 081114.
17 A. A. Patwardhan and L. A. Belfiore, *Polym. Eng. Sci.*, 1988, **28**, 916.
18 M. Pracella, B. Bresci and C. Nicolardi, *Liq. Cryst.*, 1993, **14**, 881.
19 A. Dubault, C. Casagrande and M. Veyssie, *Mol. Cryst. Liq. Cryst.*, 1982, **72**, 189.
20 S. Rucareanu, M. Maccarini, J. L. Shepherd and R. B. Lennox, *J. Mater. Chem.*, 2008, **18**, 5830.
21 M. Maccarini, G. Briganti, S. Rucareanu, X. D. Lui, R. Sinibaldi, M. Sztucki and R. B. Lennox, *J. Phys. Chem. C*, 2010, **114**, 6937.
22 H. Qi, B. Kinkead and T. Hegmann, *Adv. Funct. Mater.*, 2008, **18**, 212.

23 M. Urbanski, B. Kinkead, T. Hegmann and H.-S. Kitzerow, *Liq. Cryst.*, 2010, **37**, 1151.
24 I. Dierking, *Textures of Liquid Crystals*, Wiley-VCH Verlag GmbH & Co. KgaA, Weinhem, 2003.
25 J. Milette, V. Toader, E. R. Soule, R. B. Lennox, A. D. Rey and L. Reven, *Langmuir*, 2013, **29**, 1258.
26 G. Reitner and J. U. Sommer, *Polymer Crystallization*, Springer, Berlin, 2003.
27 F. Roussel, C. Canlet and B. M. Fung, *Phys. Rev. B: Condens. Matter Mater. Phys.*, 2002, **65**, 021701.
28 E. R. Soué and A. D. Rey, *Mol. Simul.*, 2012, **38**, 735.
29 E. R. Soulé and A. D. Rey, *Liq. Cryst.*, 2011, **38**, 201.